STEM CELLS TRANSLATIONAL MEDICINE®

TISSUE-SPECIFIC PROGENITOR AND STEM CELLS

Lung Injury Repair by Transplantation of Adult Lung Cells Following Preconditioning of Recipient Mice

IRIT MILMAN KRENTSIS,[a*] CHAVA ROSEN,[a*] ELIAS SHEZEN,[a] ANNA ARONOVICH,[a] BAR NATHANSON,[a] ESTHER BACHAR-LUSTIG,[a] NEVILLE BERKMAN,[b] MIRI ASSAYAG,[b] GUY SHAKHAR,[a] TALI FEFERMAN,[a] RAN ORGAD,[a] YAIR REISNER[a]

Key Words. Lung • Transplantation • Adult • Progenitors

[a]Department of Immunology, The Weizmann Institute of Science, Rehovot, Israel; [b]Pulmonary Medicine, Hadassah-Hebrew University Medical Center, Jerusalem, Israel

*Contributed equally.

Correspondence: Yair Reisner, Ph.D., Department of Immunology, The Weizmann Institute of Science, Rehovot, Israel. Telephone: +972-8-934-4023; e-mail: Yair.Reisner@weizmann.ac.il

Received June 8, 2017; accepted for publication October 12, 2017; first published December 20, 2017.

http://dx.doi.org/10.1002/sctm.17-0149

ABSTRACT

Repair of injured lungs represents a longstanding therapeutic challenge. We recently demonstrated that human and mouse embryonic lung tissue from the canalicular stage of development are enriched with lung progenitors, and that a single cell suspension of canalicular lungs can be used for transplantation, provided that lung progenitor niches in the recipient mice are vacated by strategies similar to those used in bone marrow transplantation. Considering the ethical limitations associated with the use of fetal cells, we investigated here whether adult lungs could offer an alternative source of lung progenitors for transplantation. We show that intravenous infusion of a single cell suspension of adult mouse lungs from GFP+ donors, following conditioning of recipient mice with naphthalene and subsequent sublethal irradiation, led to marked colonization of the recipient lungs, at 6–8 weeks post-transplant, with donor derived structures including epithelial, endothelial, and mesenchymal cells. Epithelial cells within these donor-derived colonies expressed markers of functionally distinct lung cell types, and lung function, which is significantly compromised in mice treated with naphthalene and radiation, was found to be corrected following transplantation. Dose response analysis suggests that the frequency of patch forming cells in adult lungs was about threefold lower compared to that found in E16 fetal lungs. However, as adult lungs are much larger, the total number of patch forming cells that can be collected from this source is significantly greater. Our study provides proof of concept for lung regeneration by adult lung cells after preconditioning to vacate the pulmonary niche. STEM CELLS TRANSLATIONAL MEDICINE *2018;7:68–77*

SIGNIFICANCE STATEMENT

Respiratory diseases are among the leading causes of death worldwide. Although lung surgical transplantation can offer a curative option for some of the patients, the difficulty of finding lung donors has led to an extensive search for alternative sources for transplantation. Recently, the authors showed that a single cell suspension of mouse or human fetal lung cells infused i.v. following adequate conditioning of recipient mice, led to marked lung chimerism within alveolar and bronchiolar lineages. However, considering that the use of fetal tissues is limited due to ethical constraints in many countries, this present study demonstrating lung injury repair by infusion of adults lung progenitors, paves the way for the use of adult lung cells as an alternative source for transplantation.

INTRODUCTION

Respiratory diseases are among the leading causes of death worldwide, causing more than 9 million deaths per year [1–3]. Although lung transplantation can offer a curative option for some of these patients, the difficulty of finding lung donors has led to extensive search for alternative sources for transplantation [4, 5]. Recently, we showed that fetal lung progenitors could potentially offer an attractive source for transplantation in mice provided that the lung stem cell niche in the recipient is vacated of endogenous lung progenitors by adequate conditioning [6]. Thus, in a procedure akin to bone marrow transplantation (BMT), a single cell suspension of mouse or human fetal lung cells harvested at the canalicular phase of gestation and infused i.v. following conditioning of recipient mice with naphthalene and 6 Gray total body irradiation (6 GY TBI), led to marked lung chimerism within alveolar and bronchiolar lineages. Furthermore, using a mixture of green fluorescent protein (GFP) or "tomato"-expressing donor lung cells, we found that at 6–8 weeks after transplantation, single red or green lung progenitors are capable of expanding within

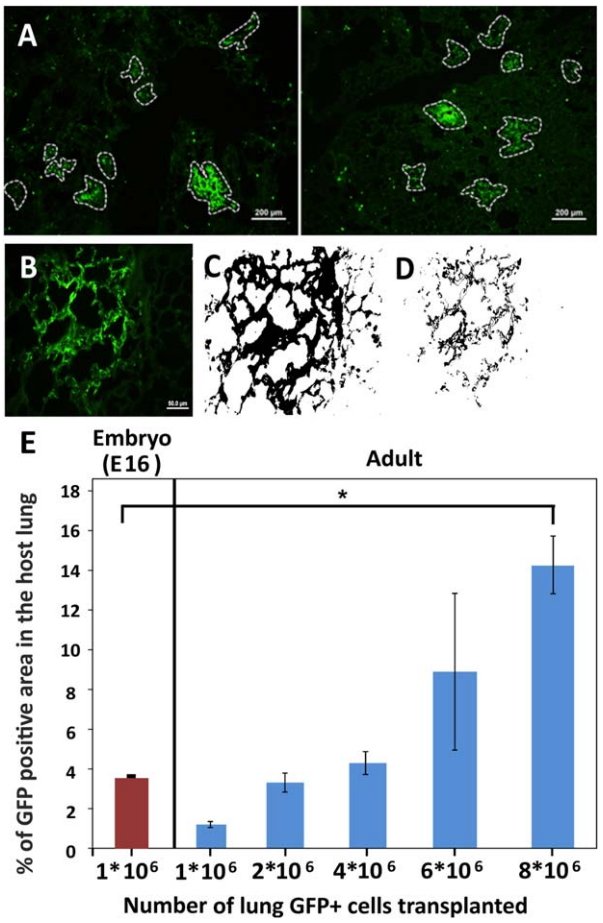

Figure 1. Morphometric analysis of lung occupancy by donor-derived cells following transplantation of different doses of lung cells. **(A):** GFP+ patches (circled) in two representative histological lung sections of recipient mice, 8 weeks after transplantation of 4E + 6 GFP+ adult lung cells following conditioning. GFP-low staining reflects auto-fluorescence of the host lung cells (scale bar = 200 μm). **(B):** A typical GFP+ patch further analyzed by Fiji software to calculate the total area of GFPhigh (donor-derived cells) plus GFPlow (autoflourescence of host cells) **(C)**, in comparison to GFPhigh only **(D)** (scale bar = 50 μm). **(E):** Percentage of the lung area occupied by GFPhigh tissue out of the total area occupied by both host GFPlow and donor GFPhigh cells. This script was used automatically on all histological pictures collected from at least seven slides, each containing three cryo-cuts with a gap of 36 microns from each other, yielding more than 1,000 micron depth into the lung tissue. Results following transplantation of different numbers of adult lung cells (Right) compared to lung occupancy after transplantation of E16 fetal lung cells (Left) ($n = 4$ mice per each group, 45–60 fields per mice). Errors bars represent mean ± SD. *t* test was used to analyze statistical significance between the E16 group and all the others. ANOVA and Dunnett's test were used to analyze statistical significance between the E16 group and all the other groups receiving adult lung cells. *, $p < .05$; **, $p < .01$; ***, $p < .001$. Abbreviations: ANOVA, analysis of variance; GFP, green fluorescent protein.

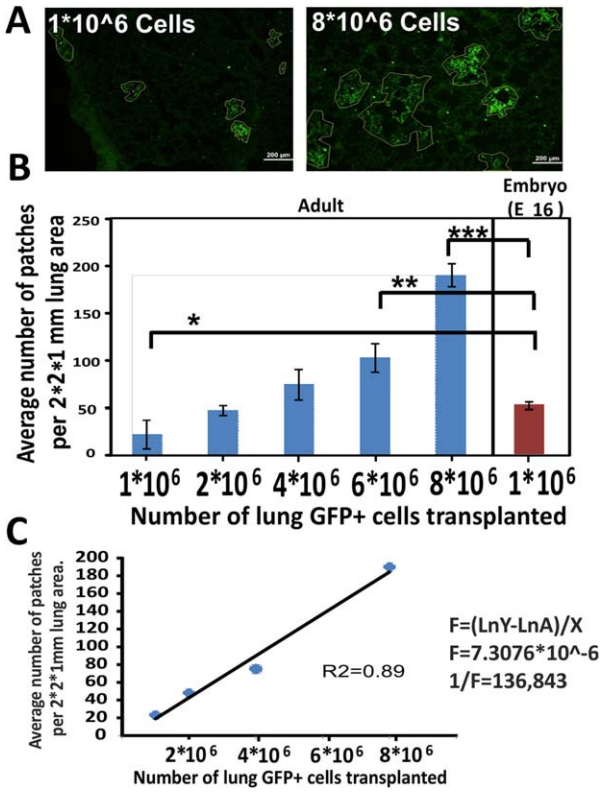

Figure 2. Patch formation following transplantation of different lung cell doses. **(A):** Typical histological sections showing GFP+ patches (circled) after transplantation of 1E + 6 or 8E + 6 adult lung cells following host conditioning (scale bar = 200 μm). **(B):** Average number of GFP+ patches in 2 × 2 × 1 mm^3 lung area of recipient mice ($n = 4$ mice per each group). Errors bars represent mean ± SD. *t* test was used in order to analyze statistical significance between the E16 group and all the others. **(C):** Linear regression of the average number of patches as a function of cell dose. The frequency of patch forming cells in adult lung cells was calculated from the slope of the line as indicated. Errors bars represent mean ± SD. ANOVA and Dunnett's test were used to analyze statistical significance between the E16 group and all the other groups. *, $p < .05$; **, $p < .01$; ***, $p < .001$. Abbreviation: ANOVA, analysis of variance.

the recipient lung to form a discrete "patch" that can be easily identified, thereby enabling quantitation of the level of "patch" forming progenitors in a given cell preparation. However, considering that the use of fetal tissues is limited due to ethical constraints in many countries, we attempted here to determine whether adult lung cells could be used as an alternative source for transplantation. While there is ample evidence from in vitro studies that different putative lung progenitors might be present in adult lungs [5–15], our recently developed novel in vivo assay for patch forming lung progenitors enabled us to further evaluate this hypothesis in the context of transplantation. Taken together, our results strongly suggest that upon adequate conditioning to vacate lung niches, a single cell suspension derived from adult lung could potentially be used instead of fetal cells for lung regeneration.

Materials and Methods

Mice

Animals were maintained under conditions approved by the Institutional Animal Care and Use Committee at the Weizmann Institute. All of the procedures were monitored by the Veterinary Resources Unit of the Weizmann Institute and approved by the Institutional Animal Care and Use Committee (IACUC). Mouse strains used included: C57BL/6J (CD45.2), β-actin-GFP (on C57BL/6J background), Rag1–/– mice on a C57BL/6J background (Weizmann breeding center), and tdTomato (Gt(ROSA)26Sortm4)

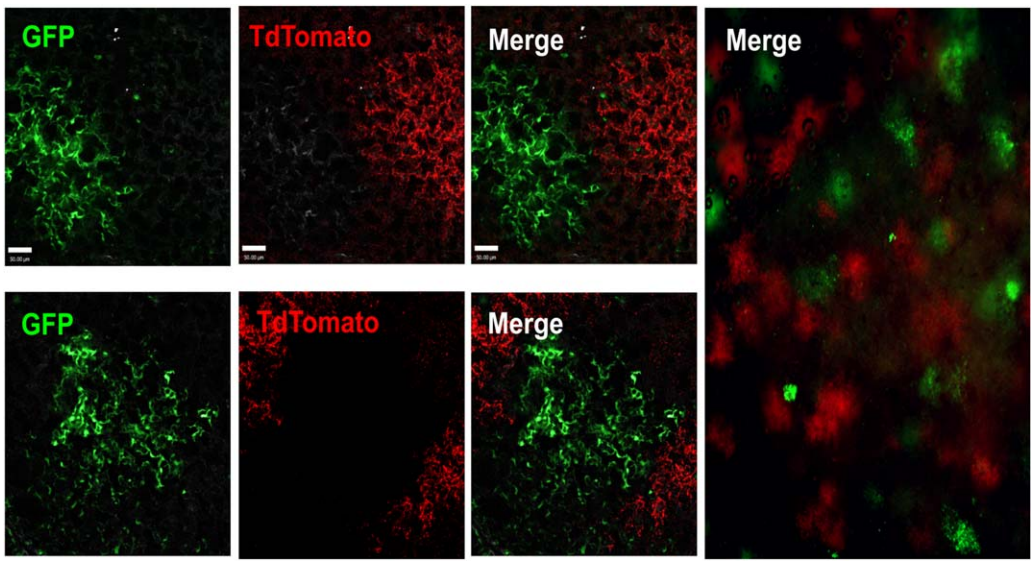

Figure 3. Three-dimensional analysis by two-photon microscopy reveals discrete green or red lung patches after transplantation of a 1:1 mixture of GFP and TdTomato lung cells. A 1:1 mixture of GFP and TdTomato adult lung cells was transplanted into recipient mice following conditioning. Mice were sacrificed and examined by two-photon microscopy 8 weeks after transfer. Discrete green or red patches were found in the host lung. The absence of yellow patches strongly indicates the clonal origin of each patch. Left: Upper and lower panels illustrate two typical fields at high magnification (extended focus image showing entire scan depth of chimeric lung; each *z* step = 1 μm, merge of 30–80 planes; scale bar = 50 μm). Right: Image of a larger field at low magnification (scale bar = 200 μm). Abbreviation: GFP, green fluorescent protein.

(ACTB-tdTomato,-EGFP) Luo/J mice (Jackson Labs, Bar Harbor, ME). All mice were used at 6–18 weeks of age. Mice were kept in small cages (up to five animals in each cage) and fed sterile food and acid water. Randomization: animals of the same age, sex, and genetic background were randomly assigned to treatment groups. Pre-established exclusion criteria were based on IACUC guidelines, and included systemic disease, toxicity, respiratory distress, refusal to eat and drink, and substantial (>15%) weight loss. During the study period, more than 90% of the mice appeared to be in good health and were included in the appropriate analysis. In all experiments, the animals were randomly assigned to the treatment groups.

For the experiment shown in Supporting Information Figure S1, C57BL/6J and C57BL/6J E16 female mice were used. For Supporting Information Figure S2, each group of five female C57BL/6J mice was used for plating 12 well plates. For Figures 1 and 2, in experiments studying dose response, conditioned C57BL/6J females, aged 8 weeks, were used as hosts, with four to five mice in each group, for two experiments. C57BL/6J–GFP female mice, aged 8–18 weeks, and E15-16–GFP positive female mice were used as lung donors. For Figures 1 and 2, seven conditioned C57BL/6J females were used as hosts, and C57BL/6J–GFP+ female mice as lung donors. For the experiment shown in Figure 3, conditioned *Rag1*$^{-/-}$-C57BL/6J female mice (aged 8–12 weeks) were transplanted with a 1:1 mixture of 6E + 6 GFP+ and tdTomato-positive adult lung cells.

For Figure 7 (lung function measurements), C57BL/6J mice were transplanted in two experiments with 4E + 6 or 6E + 6 adult lung cells from C57BL/6J–GFP+ donor mice. C57BL/6J with and without lung damage were used as controls in both experiments.

Naphthalene-Induced Lung Injury

For lung injury studies, naphthalene (>99% pure; Sigma-Aldrich) was dissolved in corn oil and administered (200 mg/kg body weight) by intraperitoneal injection, 3 days before transplantation of adult lung tissue, as previously described [16, 17]. Naphthalene-treated animals were further irradiated in an x-ray irradiator (Xrad-320), 40–48 hours after naphthalene administration, for a total dose of 6 GY TBI, and transplanted 4–24 hours later.

Mouse Adult and Fetal Lung Single Cell Suspension, Cell Preparation, and Transplantation Procedures

Cell suspensions were obtained from enzyme-digested mouse adult and embryo lungs, as previously described [18–20]. Briefly, lung digestion was performed by finely mincing tissue with a razor blade in the presence of 1 mg/ml collagenase (Roche Diagnostics, Indianapolis, IN) in phosphate buffered saline (PBS) $Ca^{+}Mg^{+}$. After incubation for 30 minutes at 37°C, an 18-G needle was used to triturate the chunks of the tissue. Following another incubation for 30 minutes at 37°C, an additional trituration with a 21-G needle was performed. Nonspecific debris were removed by sequential filtration through 100-μm filters. The cells were then washed with 1× PBS (Ca and Mg free) with 2% fetal calf serum (FCS). To prevent cell clumping before injection, 50 units heparin/ml were added to the single cell suspension before i.v. injection, and the suspension was filtered again through 40-μm filters.

Following conditioning with both naphthalene (NA) and TBI, C57BL/6J mice were transplanted with 1E + 6 to 8E + 6 GFP-positive adult or E15–16 embryo lung cells injected into the tail vein 4–24 hours following irradiation. In experiments using GFP and tdTomato labeling, *Rag1*$^{-/-}$-C57BL/6J donor mice were transplanted with a 1:1 mixture of 6E + 6 GFP- and tdTomato-positive lung cells injected into the tail vein, 4–24 hours following irradiation.

Flow Cytometry

Single cell suspensions from mouse adult and fetal lungs were prepared by enzymatic digestion and analyzed by polychromatic flow

cytometry. Samples were stained with conjugated antibodies or matching isotype controls according to the manufacturer's instructions. Antibodies were purchased from e-Bioscience, BD, and Biolegend. The complete list of antibodies used in the study is provided (Supporting Information Table S7). Data were acquired on an LSRII (BD Biosciences) or BD FACSCanto II flow cytometer, and analyzed using BD FACSDiva 6 or FlowJo software (version 7.6.5, or version vX.0.7 Tree Star, Inc.).

Immunohistochemistry

Animals were sacrificed at different time points following transplantation; the lungs were inflated to full capacity with 4% paraformaldehyde (PFA) solution and maintained for 24 hours, then cryopreserved in 30% sucrose, and snap frozen in isopentane precooled by liquid air. Frozen samples were cut into 12-μm sections and stained. The list of antibodies and dilutions used in this study is provided in Supporting Information Table S7. All secondary antibodies were purchased from Jackson Immunoresearch Laboratories or Abcam. We evaluated the stained samples using an upright Olympus BX51 fluorescent microscope with ×10, ×40 air and ×100 oil objectives, and Olympus digital camera (DP70), or by Nikon Eclipse T*i* inverted spinning disc confocal microscope with ×10, ×20 air objectives and ×40, ×60 and ×100 oil objectives for high resolution. Fluorescence microscopy images were acquired by DP Controller and DP Manager software (Olympus). Confocal microscopy images were acquired using Andor iQ software, and analyzed and reconstructed in three dimensions (as indicated) with Imaris software (Bitplane AG, Switzerland, http://www.bitplane.com). In some cases, images were processed (intensity and contrast adjusted, overlaid) in Adobe Photoshop.

Removal of CD45+ Adult Lung Cells by MACS

We prepared adult lung single cell suspensions by enzymatic digestion and in some experiments depleted CD45+ cells by Cell Separation Columns (MACS) using for positive selection (LS) columns (Miltenyi Biotec) in MACS buffer (0.5% bovine serum albumin (BSA), 2 mM EDTA in sterile 1× PBS, filtered and degassed) according to the protocol provided by the vendor. $CD45^+$ cells were depleted by treating cells by binding with anti-CD45 magnetic beads (Miltenyi Biotec). Depleted cell populations were analyzed by FACS, plated on growth factor–reduced (GFR) Matrigel (BD) for colony-forming assay as indicated in "Results" section.

In Vitro Cell Colony-Forming Assay

Epithelial cell colony-forming assay was performed according to a published protocol [18] with some modifications. Briefly, following initial isolation, lung digestion was performed by finely mincing tissue with a razor blade in the presence of 0.1% collagenase, and 2.4 U/ml dispase (Roche Diagnostics, Indianapolis, IN) in PBS Ca^+Mg^+, followed by incubation at 37°C for 30 minutes. Nonspecific debris were removed by sequential filtration through 100-μm filters. Whole lung suspensions were washed in 2% FCS in 1× PBS. Single cell suspension was either depleted of CD45 cells or sotred for CD45-Ep-Cam+ cells. The resulting single cell suspension was resuspended in 100 μl of GFR Matrigel (BD Biosciences) prediluted 1:1 (vol/vol) with epithelial colony forming units (Epi-CFU) medium and cultured in a 12 well Transwell plate (1–1.5 × 10^5 cells per well; Transwell Permeable Supports 0.4 μm, Corning), as described [18]. The absolute number of epithelial clones was determined after 7–20 days in culture. The growing clones were further characterized as described below. All cell cultures were carried out at 37°C in a 7% CO_2 humidified incubator. The medium was replaced every 48–72 hours.

Morphologic and phenotypic characterization of epithelial organoids grown in culture as described above was carried out using whole mount bright field or fluorescence immunohistochemistry. In brief, three-dimensional (3D) structures grown under culture conditions were fixed and permeabilized in a 1:1 mixture of methanol and acetone for 20 minutes at 4°C. Then, the whole mount cultures were washed briefly in 1× PBS and permeabilized and blocked using 0.5% Triton X-100 and 10% horse serum in PBS for 2 hours. Following permeabilization and blocking, the cultures were washed three times with PBS with 0.05% Tween for 20 minutes, followed by incubation with primary antibodies for 48–72 hours at 4°C. Following staining with primary antibodies, the whole mount cultures were washed with PBS and 0.5% Triton-X100 solution, and stained with relevant secondary antibodies overnight at 4°C, followed by counterstaining with Hoechst dye. Whole mount cultures were assessed by Nikon Eclipse Ti inverted spinning disc microscope. Images were acquired using Andor iQ software, and reconstructed in three dimensions with Imaris software (Bitplane AG, Switzerland, http://www.bitplane.com).

Assessment of GFP^+ Foci in Chimeric Lungs by Morphometry

Lungs were fixed with a 4% PFA solution introduced through the trachea under a constant pressure of 20 cm H_2O. Then the lungs were immersed in fixative overnight at 4°C. Lungs were processed after PFA treatment and fixed in 30% sucrose and frozen in Optimal Cutting Temperature compound (Sakura Finetek USA, Inc.Tissue-Tek.; product code #4583). Serial step sections, 12 μm in thickness, were taken along the longitudinal axis of the lobe. The fixed distance between the sections was calculated to allow systematic sampling of at least 20 sections across the whole lung. Lung slices were analyzed by fluorescence microscopy. The actual number of GFP^+ foci (a group of more than five distinct GFP^+ cells was defined as a single patch) was counted per slice using Image Pro software (Media Cybernetics, Crofton, MD, http://www.mediacy.com). The area of each slice was estimated and calculated by Fiji software (ImageJ, https://fiji.sc). The average size of each GFP+ patch was calculated, using random slices from host mice transplanted with 1E + 6 to 3E + 6 adult GFP+ lung cells, in which the GFP+ patches were distinct from one another (Figure 1). After the average GFP+ patch size was determined, the number of GFP+ patches was calculated for different cell doses (total high GFP+ area/average area of GFP+ patch [mm^2]), assuming that the frequency per area in a large number of slices reflects distribution per volume.

Calculation of GFP^+ Engrafted Area

Serial slices of chimeric lungs from different time points after transplantation were prepared and stained with anti-GFP antibody in combination with other markers as indicated in "Results" section. Serial step sections, 12 μm in thickness, were taken along the longitudinal axis of the lobe. The fixed distance between the sections was calculated to allow systematic sampling of at least 20 sections across the whole lung. Slices were obtained using Olympus fluorescent microscope and Olympus digital camera (DP70) with ×10 objective. Each analyzed image was individually evaluated for validation of the staining pattern before processing. As large GFP-positive patches containing hundreds of cells were identified in chimeric lungs, the engrafted area was calculated by Fiji

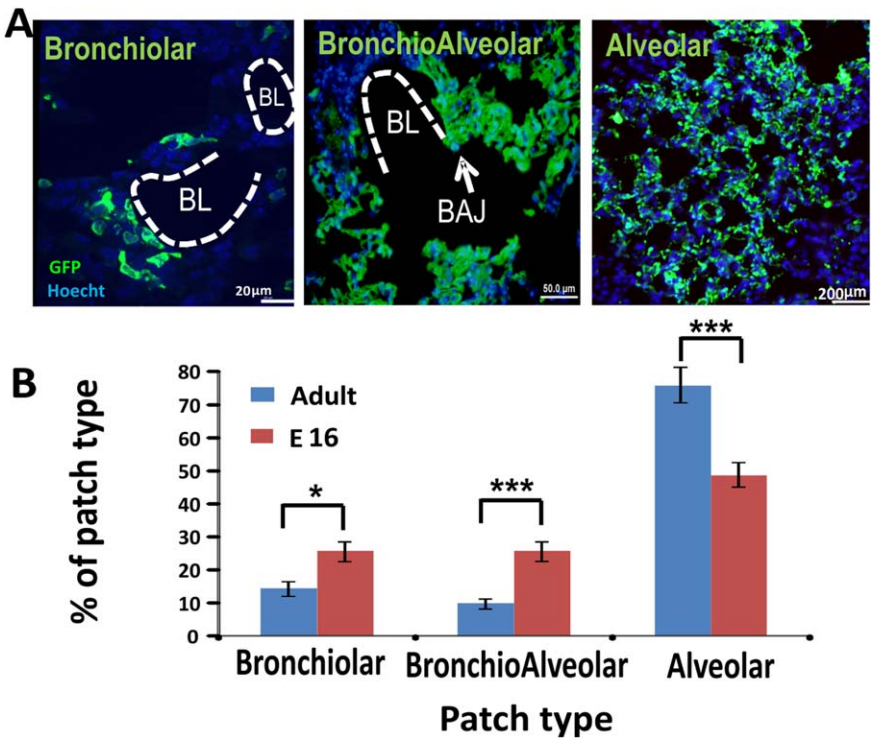

Figure 4. Different patch types found in the host lung after transplantation. Host mice were sacrificed 8 weeks post-transplantation and their lungs were evaluated by immuno-histology. **(A):** Three major types of patches were identified according to their anatomical position, namely, alveolar (scale bar = 20 μm), bronchiolar (scale bar = 50 μm), and bronchoalveolar (scale bar = 200 μm). BL and BAJ areas are bolded in the figures. Note that the GFP positive, donor derived cells, are present in both alveolar and bronchiolar regions in the host lung. **(B):** Percentage of patch types out of the total number of patches. These results ($n = 6$ mice, eight fields were counted for each mouse) were compared to results found after transplantation of 1E + 6 E16 fetal lung cells ($n = 3$ mice, 10 fields were counted for each mouse). Errors bars represent mean ± SD. *t* test was used to analyze statistical significance between the E16 and the adult groups in each section. *, $p < .05$; **, $p < .01$; ***, $p < .001$. Abbreviations: BAJ, broncho-alveolar junctions; BL, bronchiolar lumen; GFP, green fluorescent protein.

software. The green channel was extracted from the RGB image. The percentage of the engrafted area was then calculated from the whole lung tissue. Engrafted areas had high values of green intensity, whereas the whole lung tissue had low (autofluorescence) green intensity, and air space areas appeared dark. Whole lung tissue excluding air spaces filling the lung structure was detected by applying Gauss blur to the green channel (sigma = 3), setting a low fixed threshold on the blurred image and further smoothing the edges to remove small artifacts using the dilation and erosion operations. We created a mask of the whole lung tissue whose borders are illustrated in red (Figure 1) and measured its area. The RenyiEntropy global thresholding method [21] was used for calculating the intensity threshold of high GFP (engrafted) area and to create a mask whose borders are illustrated in green in Figures 3 and 4. The percentage of engrafted GFP^+ area was calculated from two measurements as high GFP^+ area (engrafted)/low GFP+ area (total tissue) × 100. In most experiments, automated software was used, but in a few instances, manual examination of the slides was required. However, in all cases, the reader was blinded to the identity of the sample.

Colocalization Analysis

Colocalization analysis was performed on fluorescent sections using Imaris 7.7.2 software (Bitplane AG, Switzerland, http://www.bitplane.com). Multiple serial slices from chimeric lungs were costained with (green) anti-GFP antibody and one of a number of markers used for colocalization analysis (always red). The images for analysis were obtained using an Olympus fluorescent microscope and Olympus digital camera (DP70) with ×40 objective. Each analyzed image was individually evaluated for validation of the pattern of the staining used before processing. The images were opened in the Imaris colocalization module, and the region of interest (ROI) for colocalization was defined by the green channel to concentrate on the relevant parts of the image, defining the whole GFP+ area as 100%. A colocalized channel was created; channel statistics were calculated and exported to Excel files. The extent of colocalization was assessed as the percentage (%) of colocalized ROI material: (total red intensity in colocalized region/total green intensity in the ROI) × 100. The data are presented as mean ± SD of all analyzed images for each marker.

Two-Photon Microscopy

Mice were euthanized before imaging. Lungs were excised and placed under a glass-covered imaging chamber. Imaging was performed using an Ultima Multiphoton Microscope (Prairie Technologies, Middleton, WI) incorporating a pulsed Mai Tai Ti-Sapphire laser (Newport Corp, CA). The laser was tuned to 850–900 nm to either excite enhanced green fluorescent protein (EGFP), or to simultaneously excite EGFP and tdTomato. A water-immersed x20 (NA 0.95) or x40 objective (NA 0.8) or x10 air objective (NA 0.3) from Olympus was used. To create a typical *z*-stack, sections of the lung containing GFP-labeled cells (the donor embryos express GFP under the β-actin promoter; thus all engrafted cells were GFP-positive) were scanned at a depth of ~30–150 μm with 1 μm

z-steps. The data were analyzed using Imaris software (Bitplane AG, Switzerland, http://www.bitplane.com). All 3D rendering of the images was performed using Imaris software.

Assessment of Airway Hyper-Responsiveness

Mice were anesthetized using ketamine/xylazine, tracheostomized, and ventilated with a FlexiVent apparatus (SCIREQ, Montreal, QC, Canada). After baseline determination of airway resistance, mice were challenged with 64 mg/ml methacholine (MCH) nebulized directly into the ventilatory circuit using an AeroNebLab nebulizer (SCIREQ). Two models of respiratory mechanics were used to assess lung resistance (R): the linear first-order single compartment model and the constant-phase model. All data points were collected with FlexiVent software (SCIREQ). Results were expressed as relative increase in R over baseline values.

Statistical Analysis

Differences between groups were evaluated by using a one-way analysis of variance (ANOVA) and Dunnett's post-test for calculating p value between the different groups compared to fetal lung results and linear regression afterward. For each data set, mean $\pm$ SD was calculated and is presented in the "Results" section of the main text. The differences between the groups were considered statistically significant for $p \leq .05$.

For dynamic lung resistance, the differences between groups were evaluated by one-way ANOVA with a priori comparisons between the groups and Dunnett's post-test. For graphical presentation of the same data sets, box plots were generated, which represent the entire data set distribution. The center line in the boxes shows the medians; box limits indicate the 25th and 75th percentiles, whiskers indicate the minimal and maximal values. The differences between the groups were considered statistically significant for $p \leq .05$.

Results

FACS Characterization of Progenitors in the Adult Mouse Lung

We first characterized the cellular composition of fetal versus adult mouse lung. As can be expected, the cell composition of the adult mouse lung was markedly different from E16 fetal lung cells (Supporting Information Fig. S1A). The adult lung exhibited higher levels of CD31+ endothelial and CD45+ hematopoietic cells, as well as of CD45- CD31- EpCam- SCA-1+ PDGR- alpha+ mesenchymal progenitors (1.9% $\pm$ 0.29% vs. 0.1% $\pm$ 0.05%) (Supporting Information Fig. S1B, S1D), while the abundance of CD45- CD31- EpCam+ CD24+ mouse epithelial progenitors (Supporting Information Fig. S1B, S1C) was much lower (1.13% $\pm$ 0.05% vs. 8.1% $\pm$ 1%).

In Vitro Differentiation of Adult Lung Cells

To evaluate the potential regenerative activity of the epithelial lung progenitors within the adult lung preparation, we initially tested their ability to form lung organoids ex vivo [18] (Supporting Information Fig. S2A). After removal of CD45+ hematopoietic cells, the remaining adult lung cells were plated on chamber plates covered with Matrigel, and 2–3 weeks later, the cultures were observed for the presence of lung organoids. The plates containing the organoids were fixed and stained for different lung differentiation markers. Although a smaller number of organoids was obtained compared to fetal lung cells, both bronchiolar-like and alveolar-like organoids could be clearly detected by light phase microscopy (Supporting Information Fig. S2B, S2C).

Notably, while epithelial cells in both types of organoids stain positive for wide spectrum cytokeratines (Supporting Information Fig. S2D, S2E), the former can be distinguished from the alveolar-like organoids by immuno-staining for Nestin depicting mesenchymal cells around the rim (Supporting Information Fig. S2D). In contrast, two photon microscopy reveals that alveolar (Supporting Information Fig. S2G) but not bronchiolar organoids (Supporting Information Fig. S2F) express SP-C, typical of surfactant producing ATII alveolar cells.

Patch Forming Capacity of Adult Lung Cells

The preliminary results described above strongly suggested, in line with previous studies [7–15], that adult lung progenitors might offer an additional source for transplantation. However, considering the limitations of ex vivo assays, it was critical to verify this possibility by using our newly developed assay for "patch" forming progenitors in vivo.

As described by Rosen et al. [6], this assay, based on transplantation of GFP+ E16 fetal lung progenitors into recipients conditioned with naphthalene and 6 GY TBI, leads to formation of discrete clonogenic patches likely derived from a single progenitor. Considering that fetal lungs exhibit approximately fourfold higher levels of CD45-CD31-Ep Cam+ cells (Supporting Information Fig. S1A), we initially chose to use a fourfold greater cell number for adult lung transplantation. Thus, we used 4E + 6 adult lung cells from C57BL-GFP donors, and we evaluated chimerism in the recipients lungs 8 weeks after transplantation. Fifth of the lung from transplanted mice was taken to FACS analysis in order to see whether we can detect GFP+ cells in the mice. Although FACS cannot be used to quantity the GFP+ cell amount, because of loss of GFP likeness from unfixed tissue, we were still able to see GFP+ cells in the host lung 8 weeks post transplantation. We also stained the lung cells for the epithelial and mesenchymal lung progenitor cells to see whether the donor cells contribute to their renewal as well. As can be seen in Supporting Information Figure S3, the cell composition of donor derived cells is similar to that found in normal lung tissue. The lung tissue were also fixed and stained in the next stage. As shown in Figure 1A, histological staining revealed GFP+ patches in the host lung, indicating that adult lung indeed contains patch forming progenitors.

In order to compare quantitatively the frequency of these patch forming progenitors in adult versus fetal lungs, we conducted a dose response experiment, in which 1E + 6 to 8E + 6 adult GFP positive cells from C57BL donor mice were transplanted after conditioning of the recipients with naphthalene, and 6 GY TBI 48 hours later. As a positive control, we administered 1E + 6 GFP fetal lung cells. Mice were sacrificed 8 weeks after transplantation, and their lungs were evaluated by immunohistology. Using the FIJI software, capable of distinguishing between different fluorescence intensities, the level of GFP intensity was recorded and analyzed throughout the lung (Fig. 1B–1E). Thus, black area in the host lung indicates the background of the scanned field, representing an empty area without cells. Weak green indicates GFP negative host cells (auto-fluorescence), while intense green staining marks donor derived GFP positive cells. The software calculation ignores the black area of the background and can estimate the percentage of the GFP high level area out of the total cellular region.

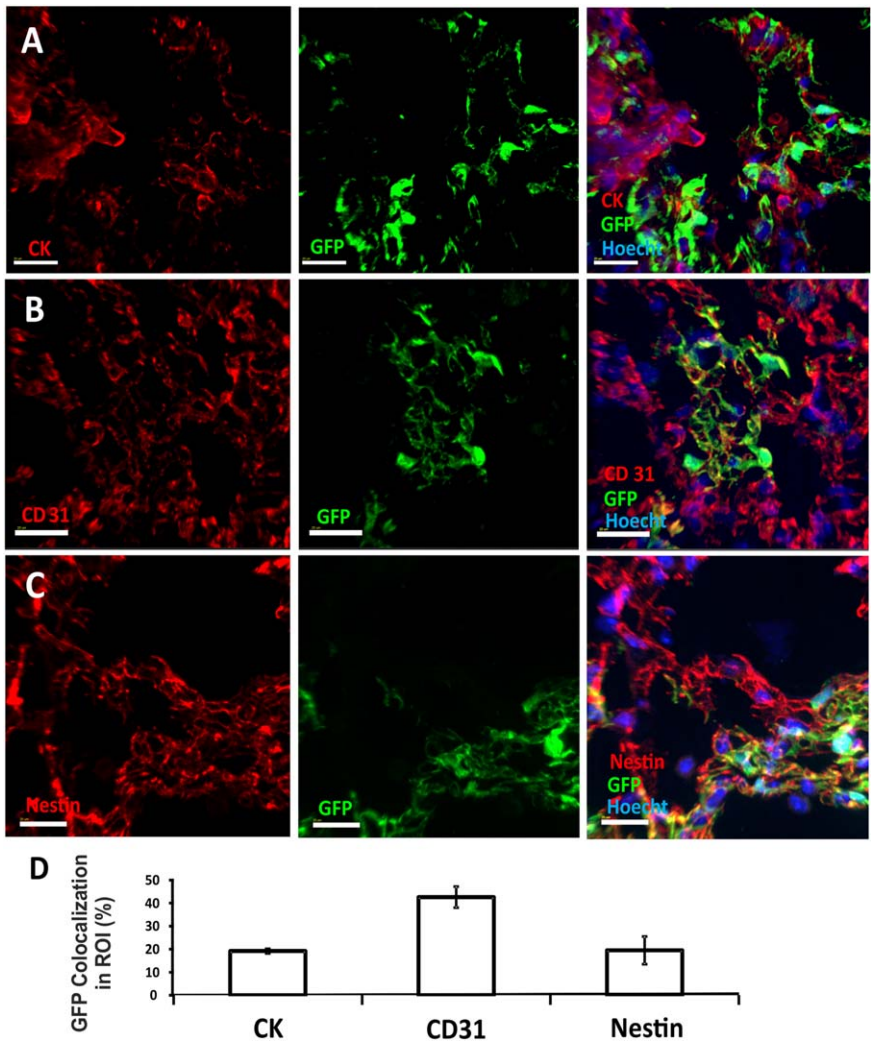

Figure 5. Different cell lineages found in GFP+ donor-derived patches. Immunohistological analysis was used to characterize the composition of donor derived GFP+ green patches. Imaris software was used to determine fluorescence colocalization. GFP+ areas were set as the area of interest, and the colocalization channel identified pixels that included both red (antibody staining) and green (donor derived cell labeling) fluorescence. Epithelial cells were stained with wide spectrum cytokeratin antibody **(A);** endothelial cells were stained with CD31 antibody **(B);** and mesenchymal cells were stained with Nestin **(C).** In each figure, the red channel represents the lineage marker, the green channel marks donor derived GFP+ cells, and the blue marks nuclear staining. Scale bar = 20 μm. **(D):** Summary of % ROI (average plus SD) colocalized 8 weeks after transplantation of 8E + 6 adult GFP+ lung cells (based on five different areas obtained from two transplanted mice). Errors bars represent mean ± SD. Abbreviations: GFP, green fluorescent protein; ROI, region of interest.

One caveat regarding this calculation is related to patch size, which increases proportionally upon cell dose escalation. Thus, at high cell doses, it becomes increasingly difficult to define the patch borders and the observed patches might include two or three neighboring patches. To address this problem, we attempted to define the average size of a single GFP patch observed at low cell dose at which single patches can be clearly delineated, and this average area was used to calculate the number of patches formed following transplantation at high cell dose. Thus, the number of patches in a total area of $2 \times 2 \times 1$ mm^3 is calculated for each lung. Again, as can be seen in Figure 2, this form of analysis showed linear dependence on cell dose.

Taken together, this analysis suggests that transplantation of about 3E + 6 adult donor lung cells results quantitatively in the same level of chimerism found following transplantation of 1E + 6 E16 fetal lung cells, indicating that the frequency of patch forming cells is about threefold lower than that found in the E16 fetal lung.

Three Dimensional Analysis by Two Photon Microscopy of Donor-Derived Patches

To visualize the integration of GFP+ donor derived cells into the 3D structure of the lung, we used two-photon microscopy, immediately after sacrifice of the transplanted mice (Supporting Information Video S4).

Notably, as previously shown for E16 lung cells, only discrete green or red without any yellow patches were found after transplantation of a 1:1 mixture of green GFP and red TdTomato positive adult lung cells (Fig. 3). Thus, 55.1% ± 7.5% of the donor derived patches were found to be TdTomato+ and 44.9% ± 7.5% were GFP+ cells, strongly indicating that each patch is derived from a single lung progenitor.

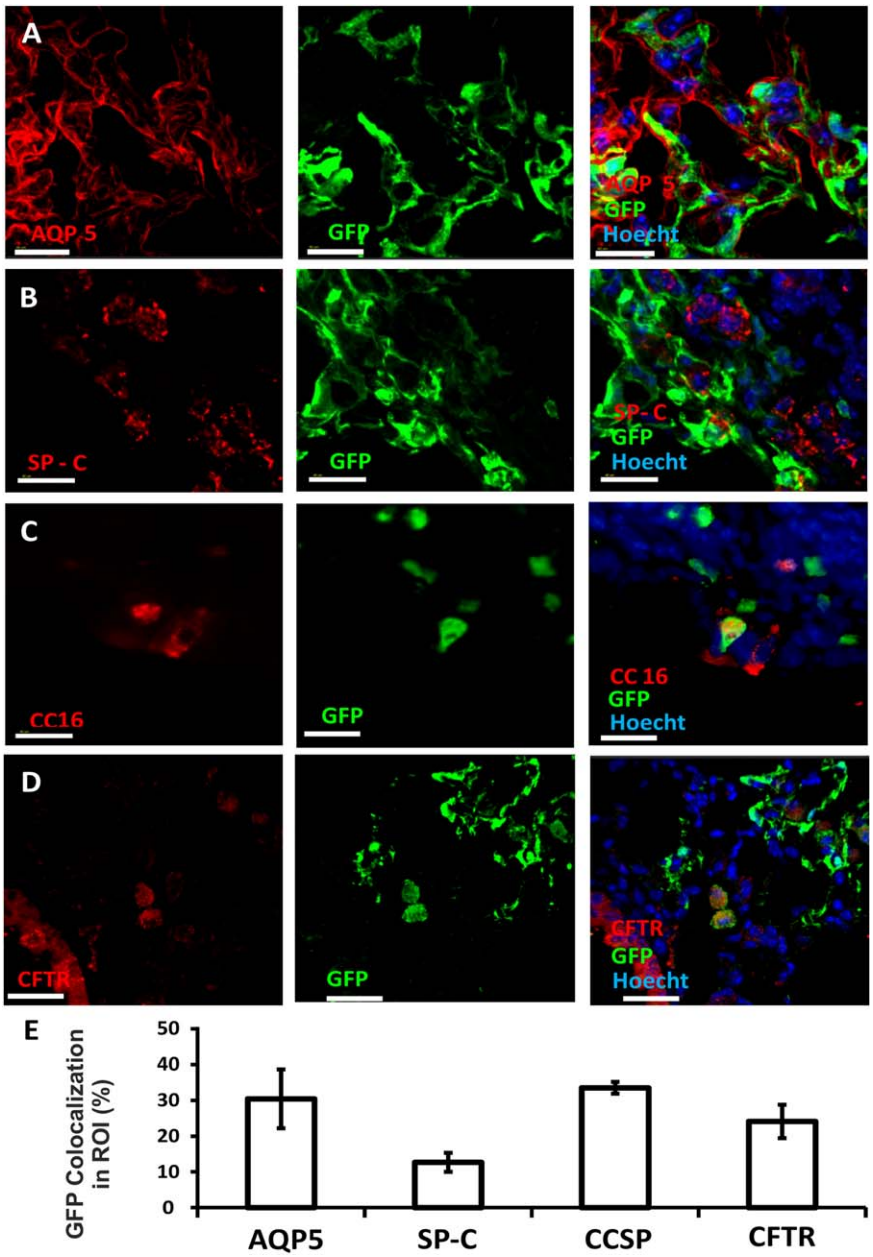

Figure 6. Integration of donor-derived cells in the epithelial lung compartment. Immunohistological analysis was used to characterize the composition of the epithelial compartment within donor-derived GFP+ green patches. Imaris software was used to determine fluorescence colocalization. GFP+ areas were designated as the areas of interest, and the colocalization channel identified pixels that included both red and green colors. ATI cells were stained with Aquaporin type 5 **(A),** ATII cells with surfactant protein C **(B),** club cells with CCSP (CC16) **(C),** and CFTR+ cells with anti-CFTR **(D).** In each figure, the red channel represents the lineage marker, the green channel marks donor-derived GFP+ cells, and the blue channel marks nuclear staining. Scale bar = 40 μm. **(E):** Summary of % ROI (average plus SD) colocalized 8 weeks after transplantation of 8E + 6 adult GFP+ lung cells (based on five different areas obtained from two transplanted mice). Abbreviations: GFP, green fluorescent protein; ROI, region of interest.

Lung Localization of Donor-Derived Patches

In general, donor derived patches can be classified by their anatomical location within the lung, namely, bronchiolar, bronchioalveolar, and alveolar patches. As can be seen in Figure 4, transplantation of adult lung cells leads predominantly to alveolar patches similarly to the results with fetal lung cells. However, bronchiolar and bronchioalveolar patches were also detected, although there was a trend for a more pronounced level of such patches following fetal lung transplantation.

Immunohistological Analysis of Donor-Derived Lung Patches

We next characterized the cell types formed within the adult lung-derived patches. As can be seen in Figure 5, immunohistological analysis revealed the presence of epithelial (CK+) (Fig. 5A and Supporting Information S5A), endothelial (CD31+) (Fig. 5B and Supporting Information S5B), and mesenchymal (Nestin+) (Fig. 5C and Supporting Information S5C) cells within each patch.

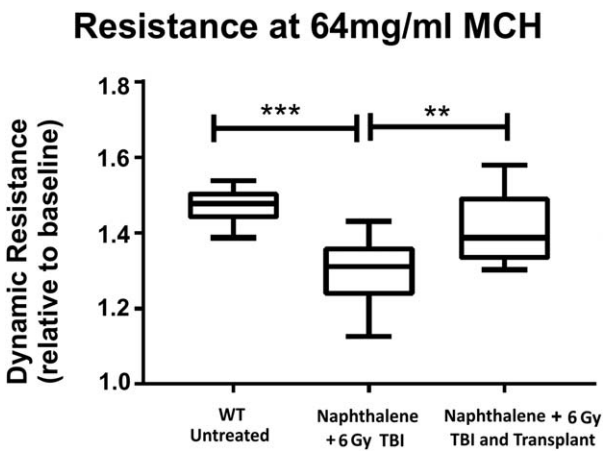

Figure 7. Dynamic lung resistance before and after adult lung transplantation. Dynamic lung resistance was measured following methacholine challenge (64 mg/ml) using the Scireq-FlexiVent instrument (Emka, France) in wild type untreated C57BL/6 mice **(A),** in mice treated with naphthalene and 6 GY TBI **(B),** and in mice treated with naphthalene and 6 GY TBI and transplanted with 4E + 6 adult lung cells **(C).** Significant differences between the three groups were established by the ANOVA and Dunnett's test ($n = 10$ in each group). Box plots show entire data distribution. Center line, median; box limits, 25th and 75th percentiles; whiskers, minimal and maximal values. *, $p < .05$; **, $p < .01$; ***, $p < .001$. Abbreviations: 6 GY TBI, 6 gray total body irradiation; ANOVA, analysis of variance; MCH, methacholine; WT, wild-type.

Within the epithelial lineage, this analysis revealed both types of differentiated alveolar cells, namely, alveolar type I (ATI) cells, responsible for gas exchange between the alveoli and the blood, and alveolar type II (ATII) cells responsible for surfactant secretion. Antibody against aquaporin 5, a major water channel expressed in ATI cells, was used to identify ATI cells (Fig. 6A and Supporting Information S6A) while surfactant protein C was used to stain ATII cells (Fig. 6B and Supporting Information S6B). Another important cell type is the Club cell, found in the bronchioles; these cells protect the bronchiolar epithelium, by secreting proteins such as uteroglobin and other components similar to surfactant. Club cells, identified by staining for the CCSP protein (CC16, Fig. 6C and Supporting Information S6C) are also responsible for detoxifying harmful substances inhaled into the lungs. Finally, as shown in Figure 6D (and Supporting Information S6D), we also found colocalization of the cystic fibrosis transmembrane conductance regulator within the GFP+ donor derived cells, indicating that, as in E16 cell transplants, the transplanted cells can potentially provide functions missing in the diseased lung of cystic fibrosis patients.

Functional Assessment of Lung Injury Repair

The marked lung colonization with donor-derived cells within different lung cell lineages strongly indicates that our transplantation procedure could offer a new modality for lung regeneration. To test the functional capacity of the transplanted cells, the dynamic resistance (R) of the lung was measured following methacholine challenge (64 mg/ml). As can be seen in Figure 7, this parameter, which quantitatively assesses the level of constriction in the lungs, was significantly reduced when tested at 8 weeks after exposure to naphthalene plus 6 GY TBI ($p = .0004$), and was completely restored when tested at the same time point after transplantation of 4E + 6 adult lung cells ($p = .0275$).

Discussion

Our group recently established that mouse and human fetal lung cells harvested at the canalicular stage of development, can successfully repair naphthalene-induced lung injury if coupled with appropriate conditioning to vacate lung stem cell niches. These findings strongly support the notion that major insights developed over the years in the area of BMT may be applicable to lung stem cell transplantation, as well. Thus, apart from stem cell competition for their respective niches, it was also shown that in analogy to the spleen colonies found following infusion of hematopoietic stem cells, which are derived from a single hematopoietic progenitor, the infusion of lung progenitors following lung injury and sublethal irradiation leads to colony-like lung patches. These patches predominantly possess characteristics of alveoli, but bronchial or bronchio-alveolar patches could also be documented. Notably, infusion of an E16 lung cell mixture (1:1) from green (GFP) and red (tomato) donors did not lead to yellow (mixed) patches, but rather, only discrete green or red patches could be detected, strongly indicating that these patches are likely derived from a single pluri-potential progenitor. Thus, while the total number of donor-derived cells might vary depending on patch size, the analysis of total number of patches as a function of cell number infused, is more meaningful, representing the relative frequency of patch-forming progenitors.

Taken together, these results offer not only a potential curative transplantation approach for the correction of lung injury, but also a new in vivo assay for lung progenitors, similar to the spleen colony assay for hematopoietic progenitors.

In our present study, we demonstrate that patch forming lung progenitors are also present in the adult lung. Colocalization analysis of fluorescence channels revealed the presence of donor-derived endothelial, epithelial, and mesenchymal cells within the patches, as well as alveolar ATI and ATII cells within alveolar patches, and CCSP+ Club cells in bronchiolar patches. Two-photon microcopy clearly documented the 3D structure of these donor-derived lung patches, and as shown for fetal lung progenitors, when using a 1:1 mixture of lung cells from green and red donors, only discrete green or red patches were observed, suggesting a single cell origin. Notably, our data not only indicate appropriate differentiation of donor derived progenitors into different epithelial lung cell types after transplantation, but also reveal marked functional repair after lung injury, as documented by measurement of lung dynamic resistance. Dose response analysis suggests that the frequency of patch forming cells in the adult lung is about threefold lower compared to that found in the fetal lung. However, considering that the adult lung tissue available for transplantation is much larger, our results suggest that the adult lung could represent a suitable alternative source to fetal lung cells, for repair of lung injury. Such cells could potentially be retrieved from cadaveric lungs or from live donors. Currently, live donor transplants require at least two lobes for minimal functionality, attained by harvest of a single lobe from each of two distinct donors. However, we envision that lung repair as opposed to lung transplantation might be effective upon Intravenous (IV) infusion of a single cell suspension of one lobe from a single live donor.

Likewise, our approach could potentially enable the use of cadaveric lung tissues found to be too small for transplantation as a whole organ. Moreover, these findings are of particular importance considering that in many countries the use of fetal tissues is forbidden or considered ethically problematic.

Conclusion

Notably, while we demonstrate the feasibility of using adult lung instead of fetal lung progenitors for lung repair, further studies are required to establish the minimal conditioning required to vacate the lung stem cell niches for successful transplantation. This may vary in different diseases depending on the occupancy of lung niches. Thus while chronic obstructive pulmonary disease (COPD) patients could potentially require minimal conditioning, we expect that achieving engraftment of donor lung progenitors in Cystic Fibrosis might require more intensive conditioning. Furthermore, considering that Naphtalene cannot be used clinically, further investigation of alternative clinically approved agents in different mouse models of lung injury or of Cystic Fibrosis are necessary.

Acknowledgments

We thank O. Golani (Weizmann Institute) for excellent assistance with the colocalization analysis and R. Rotkopf (Weizmann Institute) for his critical support with the statistical analyses. This study was supported in part by a grant from the Flight Attendant Medical Research (FAMRI), The Rambam Health Care Campus-Ernest and Bonnie Research Award for excellence in genomic medicine and by a research grant from Roberto and Renata Ruhman.

Author Contributions

I.M.K., C.R., and Y.R.: conception and design, collection and assembly of data, data analysis and interpretation, manuscript writing; I.M.K., C.R., E.S., A.A., B.N., E.B.L., M.A., T.F., and R.O.: collection and assembly of data; Y.R.: administrative support and final approval of manuscript.

Disclosure of Potential Conflicts of Interest

The authors indicated no potential conflicts of interest.

Note Added in Proof

This article was published online on 20 December 2017. Minor edits have been made that do not affect data. This notice is included in the online and print versions to indicate that both have been corrected 28 December 2017.

References

1 World Health Organization World and Europe Detailed Mortality Databases. https://www.erswhitebook.org/chapters/the-burden-of-lung-disease/.

2 Chaney J, Suzuki Y, Cantu E 3rd et al. Lung donor selection criteria. J Thorac Dis 2014;6:1032–1038.

3 Elgharably H, Shafii AE, Mason DP et al. Expanding the donor pool: Donation after cardiac death. Thorac Surg Clin 2015;25:35–46.

4 Kotton DN, Morrisey EE. Lung regeneration: Mechanisms, applications and emerging stem cell populations. Nat Med 2014;20:822–832.

5 Weiss DJ, Kolls JK, Ortiz LA et al. Stem cells and cell therapies in lung biology and lung diseases. Proc Am Thorac Soc 2008;5:637–667.

6 Rosen C, Shezen E, Aronovich A et al. Preconditioning allows engraftment of mouse and human embryonic lung cells, enabling lung repair in mice. Nat Med 2015;10:1038–3889.

7 Yee M, Domm W, Gelein R et al. Alternative progenitor lineages regenerate the adult lung depleted of alveolar epithelial type 2 cells. Am J Respir Cell Mol Biol 2016;56:453–564.

8 Henry E, Cores J, Hensley MT et al. Adult lung spheroid cells contain progenitor cells and mediate regeneration in rodents with bleomycin-induced pulmonary fibrosis. Stem Cells Translational Medicine 2014;4:1265–1274.

9 Chernaya O, Shinin V, Liu Y et al. Behavioral heterogeneity of adult mouse lung epithelial progenitor cells. Stem Cells Dev 2014;23:2744–2757.

10 McCauley KB, Hawkins F, Serra M et al. Efficient derivation of functional human airway epithelium from pluripotent stem cells via temporal regulation of Wnt signaling. Cell Stem Cell 2017;20:1–14.

11 Chimenti I, Pagano F, Angelini F et al. Human lung spheroids as in vitro niches of lung progenitor cells with distinctive paracrine and plasticity properties. Stem Cells Translational Medicine 2017;6:767–777.

12 Barkauskas CE, Chung MI, Fioret B et al. Lung organoids: Current uses and future promise. Development 2017;144:986–997.

13 Tsao P-N, Matsuoka C, Wei S-C et al. Epithelial Notch signaling regulates lung alveolar morphogenesis and airwa epithelial integrity. Proc Natl Acad Sci USA 2016;113:8242–8247.

14 Jain R, Barkauskas CE, Takeda N et al. Plasticity of Hopx+ type I alveolar cells to regenerate type II cells in the lung. Nat Commun 2015;6:6727–6746.

15 Trecartin A, Danopoulos SD, Spurrier R et al. Establishing proximal and distal regional identities in murine and human tissue-engineered lung and trachea. Tissue Eng Part C Methods 2016;22:1049–1057.

16 Stripp BR, Maxson K, Mera R et al. Plasticity of airway cell proliferation and gene expression after acute naphthalene injury. Am J Physiol 1995;269:791–799.

17 Wong AP, Keating A, Lu W-Y et al. Identification of a bone marrow–derived epithelial-like population capable of repopulating injured mouse airway epithelium. J Clin Invest 2009;119:336–348.

18 Bertoncello I, McQualter J. Isolation and clonal assay of adult lung epithelial stem/progenitors cells. Curr Protoc Stem Cell Biol 2011;16:2G.1.1–2G.1.12.

19 Liang SX, Summer R, Sun X et al. Gene expression profiling and localization of Hoechst-effluxing $CD45^{-}$ and $CD45^{+}$ cells in the embryonic mouse lung. Physiol Genomics 2005;23:172–181.

20 Summer R, Kotton DN, Liang S et al. Embryonic lung side population cells are hematopoietic and vascular precursors. Am J Respir Cell Mol Biol 2005;33:32–40.

21 Kapur JN, Sahoo PK, Wong AKC. A new method for gray-level picture thresholding using the entropy of the histogram. Comput Vis Graph Image Process 1985;29:273–285.

See www.StemCellsTM.com for supporting information available online.